



An edge-based smoothed point interpolation method (ES-PIM) for heat transfer analysis of rapid manufacturing system

S.C. Wu^{a,b,*}, G.R. Liu^{b,c}, X.Y. Cui^{b,d}, T.T. Nguyen^c, G.Y. Zhang^c

^a Centre for Advanced Materials Joining & Simulations (AMJS), School of Materials Science and Engineering, Hefei University of Technology, Hefei 230009, PR China

^b Centre for Advanced Computations in Engineering Science (ACES), Department of Mechanical Engineering, National University of Singapore, 117576 Singapore, Singapore

^c Singapore-MIT Alliance (SMA), E4-04-10, 4 Engineering Drive 3, 117576 Singapore, Singapore

^d State Key Laboratory of Advanced Design and Manufacturing for Vehicle Body, Hunan University, Changsha 410082, PR China

ARTICLE INFO

Article history:

Received 21 July 2009

Received in revised form 3 December 2009

Accepted 3 December 2009

Available online 22 January 2010

Keywords:

Numerical methods

Meshfree method

Transient heat transfer

Gradient smoothing

Point interpolation method

Rapid plasma deposition dieless

manufacturing

ABSTRACT

This paper formulates an edge-based smoothed point interpolation method (ES-PIM) for analyzing 2D and 3D transient heat transfer problems with mixed boundary conditions and complicated geometries. In the ES-PIM, shape functions are constructed using the polynomial PIM with the Delta function property for easy treatment of essential boundary conditions. A generalized smoothing technique is used to reconstruct the temperature gradient field within the edge-based smoothing domains. The generalized smoothed Galerkin weak form is then used to establish the discretized system equations. Our results show that the ES-PIM can provide more close-to-exact stiffness compared with the “overly-stiff” finite element method (FEM) and the “overly-soft” node-based smoothed point interpolation method (NS-PIM). Owing to this important property, the present ES-PIM provides more accurate solutions than standard FEM using the same mesh. As an example, a practical cooling system of the rapid direct plasma deposition dieless manufacturing is studied in detail using the present ES-PIM, and a set of “optional” processing parameters of fluid velocity and temperature are found.

© 2009 Elsevier Ltd. All rights reserved.

1. Introduction

The finite element method (FEM) is currently the most popular numerical approach to obtain approximate solutions for practical heat transfer systems [1–3]. However, the well-known “overly-stiff” property of fully-compatible FEM based on the element mesh results in solutions with lower temperature, and may result loss in significant accuracy for temperature gradient [4,5]. To solve this problem, meshfree methods [6–9] have been developed with remarkable progress in analyzing engineering heat transfer problems, such as the element-free Galerkin method (EFG) [10,11], the meshless local Petrov-Galerkin method (MLPG) [12], the smoothed particle method (SPH) [13], the point interpolation method (PIM) [14–16], etc.

A node-based smoothed PIM (NS-PIM or LC-PIM originally) has been proposed for mechanics problems [7] and then used to analyze steady heat transfer and thermoelastic problems [14–16]. The NS-PIM employs the PIM shape functions constructed using a small set of nodes in a local support domain [17], and the gener-

alized gradient smoothing operation [18] that was proposed based on the node-based smoothing technique [19]. Compared with the “over-stiff” FEM model using three-node triangular cells, the NS-PIM is found very stable (spatially), and can produce much better gradient solution. It works well with triangular [7] and tetrahedral [14,15,20] types of mesh. It is also free from volumetric locking, and capable of producing the important upper bound solutions for “force-driving” problems when not-too-coarse mesh is used. All these important properties are mainly due to the *softening* effect induced to the stiffness of the structure, as discovered in [21]. A theoretical study and an intensively numerical investigation on the upper bound of NS-PIM can be found in Ref. [21].

Based on the idea of NS-PIM, a node-based smoothed FEM (NS-FEM) [22] has also been formulated in the framework of FEM settings. The NS-FEM can be viewed as a special case of the NS-PIM, and the *n*-sided polygonal cell meshes can be used. NS-FEM always uses compatible displacement fields created based on cells, and has quite similar properties as NS-PIM that allows incompatible displacement fields [8]. By combining the FEM procedure and the gradient smoothing operation, a smoothed FEM (or SFEM) [23] has also been formulated recently and then applied for problems of plate and shells [24]. It works very effectively for solid mechanics and *n*-sided polygonal cells and very heavily distorted mesh can be used [25]. Detailed theoretical aspects including stability and

* Corresponding author. Address: Centre for Advanced Materials Joining & Simulations (AMJS), School of Materials Science and Engineering, Hefei University of Technology, Hefei 230009, PR China. Tel.: +86 159 56927120; fax: +86 551 2901362.

E-mail address: wushengchuan@gmail.com (S.C. Wu).

Nomenclature

div	divergence operator
grad	gradient operator
h	convection heat coefficient, $W/(m^2 \text{ } ^\circ\text{C})$
k	heat conductivity, $W/(m \text{ } ^\circ\text{C})$
Q_v	internal heat source, W/m^3
q_r	prescribed heat flux on 2nd boundary
T_a	temperature of ambient medium, $^\circ\text{C}$
T_r	known temperature on 1st boundary, $^\circ\text{C}$
\mathbf{x}	Cartesian coordinate
w	weighted test function

Greek symbols

Φ	vector of the PIM shape functions
φ	PIM shape function

Γ	domain boundary
Ω	problem domain studied
Δ	time spacing variation

Subscripts

e	equivalent heat transfer coefficient, $W/(m^2 \text{ } ^\circ\text{C})$
T	equivalent energy in Eq. (29)
k	smoothing area and volume

Superscripts

T	transpose operator
h	convection matrix
b	specified bulk temperature, $^\circ\text{C}$

convergence about SFEM can be found in [26]. The study of SFEM has also clearly shown that the smoothing operation on strains controls the assumed strain field in a proper fashion to ensure the stability and convergence, and ultimately gives it excellent features. However, it is found that both the NS-PIM and NS-FEM cannot solve time-dependent problems [14–16,20–22] due to their “overly-softness” of system induced by the excessive node-based smoothing operations. It is this type of overly-smoothing that leads to temporal instability (observed as spurious energy eigenmodes) for solving dynamic problems.

To overcome the temporal instability problems mentioned above, methods using edge-based smoothing domains have been developed in both FEM and meshfree settings, i.e., edge-based smoothed FEM (ES-FEM) [27–29], face-based smoothed FEM (FS-FEM) [30] and edge-based smoothed PIM (ES-PIM) [9], and cell-based smoothed PIM (CS-PIM) [31,32]. The stability and convergence of these methods are ensured by the G space theory [33]. The solutions of ES-FEM and FS-FEM are much more accurate in both the primary variable and its gradient than those of FEM models, and even more accurate solutions can be obtained compared with those of the FEM using quadrilateral cells with the same set of nodes for the 2D solid mechanics problems [27]. They are both partially and temporally stable, have no spurious modes, and hence would work well for transient dynamic problems.

In manufacturing processes of rapid heating and solidification, it is practically important to study the thermal behaviors of the products to ensure the quality and performance. Engineers are particularly interested in the temperature distribution and especially the maximum temperature gradients and stress components at the critical zone and time [31]. Numerical means such as the FEM is mostly preferred for this kind of studies so far, because an experimental study is usually very expensive, time-consuming and difficult to conduct properly. Furthermore, due to the “overly-stiff” property of FEM model, significant errors occur in the temperature field especially in high gradient regions. A full-compatible FEM model also offers a lower bound solution in temperature. In contrasts, the “soft” nature of a NS-PIM model offers a useful complementary property of upper bound solution and much better gradient solutions [21]. Thus a simple combination of the upper bound NS-PIM and the lower bound FEM can bound the numerical solutions from both sides for realistic complicated thermal problems as long as a reasonably fine background mesh can be created [8].

In solving multi-dimensional problems with complicated geometries, meshing has always been a very important issue [6]. It is the opinion of the authors’ group that the ultimate solution to these thermal systems is to use triangular and tetrahedral types of meshes. Many meshfree methods and cell-based methods

enhanced by meshfree techniques [22,27] have been thus formulated based on this consideration.

In this work, two numerical approaches for ES-PIM in two-dimensions and a face-based smoothed PIM (FS-PIM) in three-dimensions are formulated to analyze transient heat transfer problems with complicated geometry and boundary conditions. In the formulation, we use the elements of triangle and tetrahedron that can be generated automatically for 2D and 3D analyses. For the convenience in presentation, both ES-PIM and FS-PIM are generally referred as ES-PIM. PIM shape functions [6] are constructed using polynomial basis and a set of small supporting nodes. Discretized system equations for transient heat transfers are formulated using the generalized smoothed Galerkin weak form [18]. The accuracy in temperature and the convergence in equivalent energy are studied and compared with those obtained using the “overly-stiff” FEM and the “overly-soft” NS-PIM [21]. Finally, a real cooling system of the rapid direct manufacturing is evaluated to find out the optimal temperature and velocity of the cooling water needed in the manufacturing process ensuring product quality.

2. PIM shape functions

The PIM shape functions can be created using both polynomial [17] and radial function bases [33,34]. The polynomial PIM is a series approximate scheme to create meshfree shape functions, using a small set of nodes within a local support [7]. In the scheme, the problem domain is first discretized with the triangles and tetrahedrons that can be automatically generated using any standard routine available for 2D and 3D solid structures. Then a set of smoothing domains $\Omega_{\mathbf{x}}$ associated with each edge (face) of the background cells are constructed based on the constant strain mesh.

Consider a function $T(\mathbf{x}, t)$ defined in the problem domain $\Omega_{\mathbf{x}}$ bounded by $\Gamma_{\mathbf{x}}$,

$$T^h(\mathbf{x}, t) = \sum_{i=1}^n p_i(\mathbf{x}) a_i = \mathbf{p}^T(\mathbf{x}) \mathbf{a}(\mathbf{x}, t) \quad (1)$$

where $\mathbf{p}(\mathbf{x})$ is the monomial basis function, n is the number of nodes inside the local support domain, a is the time-dependent coefficients yet to be determined.

To construct PIM shape functions using polynomial basis, it is well known that moment matrix may be singular [6]. A T-scheme has been proposed to select the supporting nodes for interpolation of points of interest in cells [9]. As illustrated in Fig. 1, when the interested \mathbf{x} is located in an interior cell, we select six nodes: three nodes of the home cell (j_1 – j_3) and another three at the remote

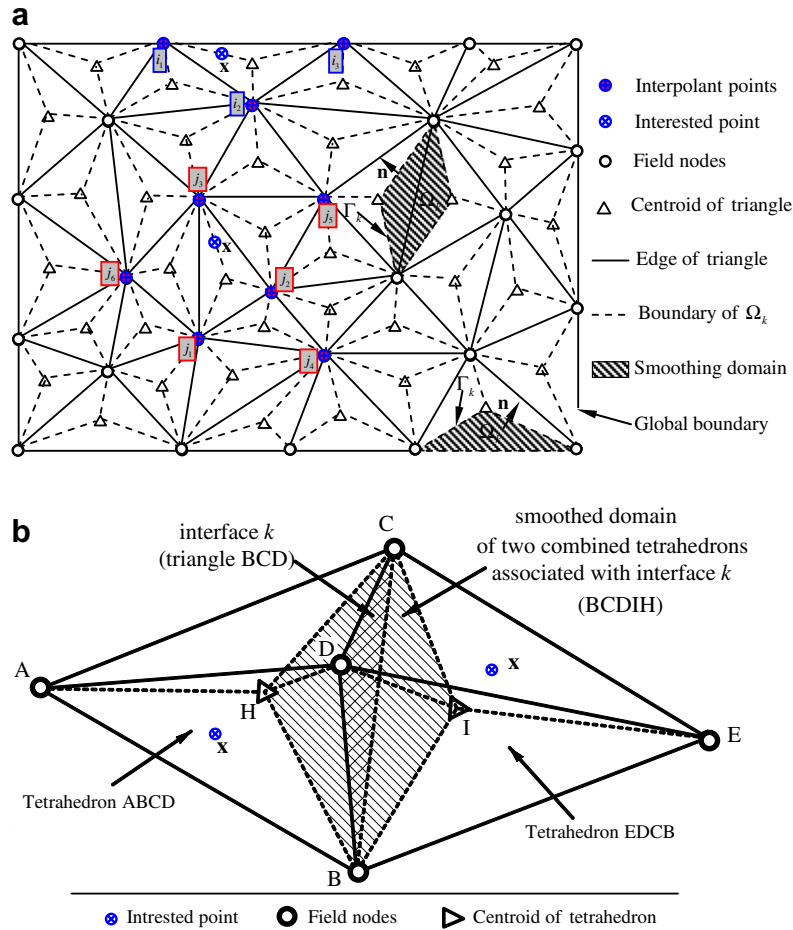


Fig. 1. Illustration of constructing smoothing domains for 2D and 3D problems. (a) 2D edge-based smoothing domains created by sequentially connecting the centroids of adjacent triangles to end-points of the edge (edge k). (b) 3D face-based smoothing domains (shaded domain) created by connecting the centroids of two adjacent tetrahedrons to vertexes of the surface triangle (face k).

vertices of three neighboring cell (j_4-j_6). When \mathbf{x} is in a boundary cell, only three vertices are selected as the interpolant nodes (i_1-i_3). This nodes selection leads to the quadratic ES-PIM (T6/3 scheme). For linear interpolations, three nodes of the triangular cell hosting \mathbf{x} are selected for all cells, which leads to the linear ES-PIM (T3 scheme).

This selection scheme is purposely devised for creating different PIM shape functions, where quadratic interpolations are performed for the interior cells and linear interpolations for boundary cells. It not only successfully overcomes the singular problem in the process of polynomial PIM shape functions construction, but also improve the efficiency [9]. More importantly, the use of three nodes for boundary cells insures the pass of the standard patch tests.

For three-dimensional cases with linear interpolation (which is in fact the same as the FS-FEM [30]), we simple select four nodes of the home cell hosting \mathbf{x} . No matter the interested point of \mathbf{x} located in an interior or a boundary cell, only the four vertexes of the home cell are selected leading to linear FS-PIM (T4). Note that the linear PIM shape functions so constructed are exactly the same as those in standard FEM using linear tetrahedral cells and then used to interpolate the unknown temperature field. The PIM shape functions can always be constructed and the moment matrix will never be singular [6], as long as these four nodes are not in the same plane. Alternative schemes for construct PIM shape functions can be found in [9].

The basis $\mathbf{p}(\mathbf{x})$ in Eq. (1) can usually be built using the Pascal's triangles and a complete lower order basis is generally preferred.

For two-dimensional problems, the complete polynomial basis of orders 1 and 2 can be written as

$$\begin{aligned} \mathbf{p}^T(\mathbf{x}) &= \{ 1 \quad x \quad y \} \\ \mathbf{p}^T(\mathbf{x}) &= \{ 1 \quad x \quad y \quad x^2 \quad xy \quad y^2 \} \end{aligned} \quad (2)$$

and for three-dimensional problems studied in this paper we only use the linear basis

$$\mathbf{p}^T(\mathbf{x}) = \{ 1 \quad x \quad y \quad z \} \quad (3)$$

The coefficients in Eq. (1) can be determined by enforcing the temperature function to be satisfied at the n nodes within the local support domain, and then we obtain the approximated field function as

$$T^h(\mathbf{x}, t) = \sum_{i=1}^n \varphi_i(\mathbf{x}) T_i(t) = \Phi^T(\mathbf{x}) \mathbf{T}(t) \quad (4)$$

where $\mathbf{T}(t)$ is the nodal parameters and $\Phi(\mathbf{x})$ are

$$\Phi^T(\mathbf{x}) = \{ \varphi_1(\mathbf{x}) \quad \varphi_2(\mathbf{x}) \quad \cdots \quad \varphi_n(\mathbf{x}) \} \quad (5)$$

The derivatives of the PIM shape function can be obtained very easily due to its polynomial property, but they are *not* required in the present ES-PIM and FS-PIM based on the weakened weak (W^2) formulation [8]. In addition, shape functions created using the PIM procedure possess the Delta function property, which permits simple treatment of essential boundary conditions just as what we do in the FEM.

Note that when high order polynomial PIM or RPIM shape functions [35–39] are used, the displacement field is not compatible and the generalized smoothing technique [18] needs to be used. The theoretical foundation for such a formulation is the G space theory [33] leading to the W^2 form that guarantees stability and the convergence to the exact solution [8]. In this work, we adopt both linear and quadratic interpolations for ES-PIM and only linear interpolation for FS-PIM, respectively, based on the background triangular and tetrahedral mesh for 2D and 3D problems.

3. Detailed formulation of the ES-PIM

3.1. Strong form equations

For transient heat transfer problems in a single material with domain Ω bounded by Γ , our problem is to find $T(\mathbf{x}, t)$ that satisfies the following equations [1,40]:

$$\text{div}(k \text{grad} T) + Q_v = \rho c \frac{\partial T}{\partial t} \quad \text{for } \mathbf{x} \text{ in } \Omega, \quad t > 0 \quad (6)$$

$$T = T_r \quad \text{for } \mathbf{x} \text{ on } \Gamma_1, \quad t > 0 \quad (7)$$

$$-(k \text{grad} T) \cdot \mathbf{n} = -k \frac{\partial T}{\partial n} = q_r \quad \text{for } \mathbf{x} \text{ on } \Gamma_2, \quad t > 0 \quad (8)$$

$$-(k \text{grad} T) \cdot \mathbf{n} = -k \frac{\partial T}{\partial n} = h(T - T_b) \quad \text{for } \mathbf{x} \text{ on } \Gamma_3, \quad t > 0 \quad (9)$$

$$-(k \text{grad} T) \cdot \mathbf{n} = -k \frac{\partial T}{\partial n} = 0 \quad \text{for } \mathbf{x} \text{ on } \Gamma_4, \quad t > 0 \quad (10)$$

$$T = T_{\text{ini}} \quad \text{for } \mathbf{x} \text{ in } \Omega, \quad t = 0 \quad (11)$$

where ρ is the density, c is the specific heat, \mathbf{n} is the unit normal vector, and T_{ini} is the initial temperature.

3.2. Standard Galerkin weak form

To find an approximate solution over time and space domain using the standard Galerkin procedure, the space of test functions is define as

$$V = \{w(\mathbf{x}) | w = 0 \text{ on } \Gamma_1; \quad w \in C^0(\Omega)\} \quad (12)$$

By multiplying Eq. (6) with a test function $w \in V$ and using the Divergence Theorem, we obtain the variational formulation

$$\begin{aligned} & \int_{\Omega} \left[k \text{grad} T \cdot \text{grad} w + \rho c \frac{\partial T}{\partial t} w \right] d\Omega \\ & = \int_{\Omega} Q_v w d\Omega - \int_{\Gamma_2} w q_r d\Gamma - \int_{\Gamma_3} w h(T - T_b) d\Gamma \end{aligned} \quad (13)$$

Substituting Eq. (4) into Eq. (13), and set φ_i as the test function w , we have the following discrete set of N total unknowns of temperature equations:

$$[\mathbf{K} + \mathbf{K}^c] \{\mathbf{T}\} + [\mathbf{M}] \{\dot{\mathbf{T}}\} = \{\mathbf{F}\} \quad (14)$$

in which

$$\mathbf{K}_{ij} = \int_{\Omega} \begin{bmatrix} \Phi_{i,x} \\ \Phi_{i,y} \\ \Phi_{i,z} \end{bmatrix}^T \begin{bmatrix} k_x & 0 & 0 \\ 0 & k_y & 0 \\ 0 & 0 & k_z \end{bmatrix} \begin{bmatrix} \Phi_{j,x} \\ \Phi_{j,y} \\ \Phi_{j,z} \end{bmatrix} d\Omega \quad (15)$$

$$\mathbf{K}_{ij}^c = \int_{\Gamma_3} h \Phi_i^T \Phi_j d\Gamma \quad (16)$$

$$\mathbf{M}_{ij} = \int_{\Omega} \rho c \Phi_i^T \Phi_j d\Omega \quad (17)$$

$$\mathbf{F}_i = \int_{\Omega} \Phi_i^T Q_v d\Omega - \int_{\Gamma_2} \Phi_i^T q_r d\Gamma + \int_{\Gamma_3} h T_b \Phi_i^T d\Gamma \quad (18)$$

where the superscript c denotes the convection heat transfer matrix, \mathbf{K} represents the conductance (or usual “stiffness”) matrix, \mathbf{M}

is the capacitance matrix, and the superposed dot of nodal temperature vector \mathbf{T} indicates the time differentiation. Note that here \mathbf{M} is adopted as the “lumped” mass matrix, which shows superiority over the consistent mass matrix especially in dynamics and nonlinear problems [3]. The above-mentioned standard Galerkin weak form leads to a FEM model.

3.3. Generalized smoothed Galerkin weak form

In the generalized smoothed Galerkin (or GS-Galerkin) weak formulation, the compatible temperature gradient shown in Eq. (13) will be replaced by a reconstructed gradient field using the generalized smoothed gradient over smoothing domains [8,18]. Naturally the integration of conductance matrix is based on the smoothing domains Ω_k ($k = 1, 2, \dots, N$), where N is the total number of edges or faces, respectively, in the 2D or 3D problems domains. Using this set of edge- and face-based smoothing domains, the domain integration in Eq. (15) becomes simple summation, and the standard “stiffness” matrices are transformed into the smoothed conductance matrices

$$\bar{\mathbf{K}}_{ij} = \sum_{k=1}^N \bar{\mathbf{K}}_{ij}^{(k)} \quad (19)$$

in which the summation implies “assembly”, and

$$\bar{\mathbf{K}}_{ij}^{(k)} = \int_{\Omega_k} \bar{\mathbf{B}}_i^T \mathbf{k} \bar{\mathbf{B}}_j d\Omega \quad (20)$$

The generalized gradient smoothing technique that works also for discontinuous field functions [18] is now applied over the smoothing domain to obtain the smoothed gradient for the interested node \mathbf{x}_k

$$\bar{\mathbf{g}}_i(\mathbf{x}_k) = \frac{1}{V_k} \int_{\Gamma_k} T n_i d\Gamma \quad (21)$$

where Γ_k is the boundary of Ω_k , n_i is the i th component of the outwards normal on Γ_k , and T is the assumed temperature field in a proper G space. It is shown that the gradient of the temperature field is not used in our formulation and the T can be discontinuous in Ω_k , so long it is continuous on Γ_k .

In Eq. (22), V_k is the area in two-dimensions or volume in three-dimensions of smoothing domain Ω_k of edge or face k that can defined by

$$V_k = \int_{\Omega_k} d\Omega = \frac{1}{3} \sum_{j=1}^{N_e^k} A_e^{(j)} \quad \text{for 2D problems} \quad (22)$$

$$V_k = \int_{\Omega_k} d\Omega = \frac{1}{4} \sum_{j=1}^{N_e^k} V_e^{(j)} \quad \text{for 3D problems} \quad (23)$$

where N_e^k is the number of cells around the edge or face k ($N_e^k = 1$ for the boundary edges or faces and $N_e^k = 2$ for interior edges or faces), $A_e^{(j)}$ and $V_e^{(j)}$ are the area and volume of the j th cell around the edge and face k , respectively.

Using PIM shape functions to construct the field function for temperature, the smoothed gradient for node k can be written in the following matrix form

$$\bar{\mathbf{g}}(\mathbf{x}_k) = \sum_{l \in D_k} \bar{\mathbf{B}}_l^{Q_k} \mathbf{T}_l \quad (24)$$

where D_k is the set of nodes used in the interpolation for field function on Γ_k .

For three-dimensional spaces, the corresponding forms are given by

$$[\bar{\mathbf{B}}_I^{\Omega_k}]^T = [\bar{b}_{I1} \quad \bar{b}_{I2} \quad \bar{b}_{I3}] \quad (25)$$

$$\bar{b}_{Ip} = \frac{1}{V_k} \int_{\Gamma_k} \varphi_I(\mathbf{x}) n_p(\mathbf{x}) d\Gamma \quad (p = 1, 2, 3) \quad (26)$$

where $\varphi_I(\mathbf{x})$ is the PIM shape function for node I .

Using Gauss integration along each sub-boundary edge or surface Γ_k of the smoothing domain Ω_k , Eq. (26) can be rewritten in the following summation form as

$$\bar{b}_{Ii} = \frac{1}{V_k} \sum_{q=1}^{N_s} \left[\sum_{r=1}^{N_g} w_r \varphi_I(\mathbf{x}_{qr}) n_i(\mathbf{x}_q) \right] \quad (27)$$

where N_s is the number of sub-boundary edge or surface of Γ_k , N_g is the number of total Gauss points located in each Γ_k , w_r is the corresponding weight of given Gauss points.

Eq. (27) implies that only shape function values at points are needed and no explicit analytical form of shape functions is required. This gives tremendous freedom in the shape function construction, and the shape functions need not to be formed explicitly. Function values at interested points can be obtained by simple interpolation.

The smoothed Galerkin weak form can be obtained by replacing the conductance matrix \mathbf{K} in Eq. (14) with the following smoothed “stiffness” matrix

$$\bar{\mathbf{K}}_{ij}^{(k)} = [\bar{\mathbf{B}}_I^{\Omega_k}]^T \mathbf{k} [\bar{\mathbf{B}}_I^{\Omega_k}] V_k \quad (28)$$

It can be easily seen from Eq. (28) that the resultant linear system is symmetric and banded (due to the compact supports of PIM shape

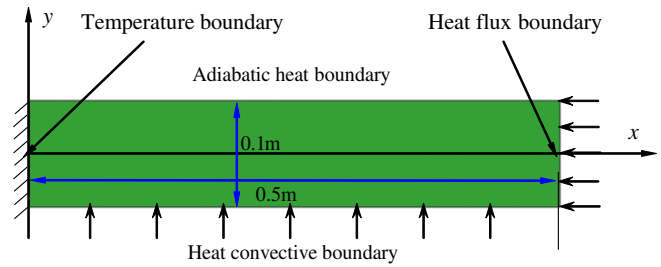


Fig. 2. Schematics of 2D transient problem.

functions). In addition, we only modify the “stiffness” matrix in Eq. (15) by the smoothed Eq. (20), which can solve the smoothed Galerkin weak form efficiently.

4. Results and discussions

For solving the transient response, the discretized equation system from the GS-Galerkin weak form is a set of differential equations that require further discretized using Crank-Nicolson difference technique in time domain [3]. Both the 2D and 3D codes have been developed in FORTRAN, and a direct Gaussian elimination solver [41] is used to analyze the transient heat transfer problems. For comparison, both the FEM and NS-PIM in-house codes are also developed to evaluate the same problems using the exactly same solver and meshes. The critical time step Δt can be determined in terms of the maximum generalized eigenvalue of

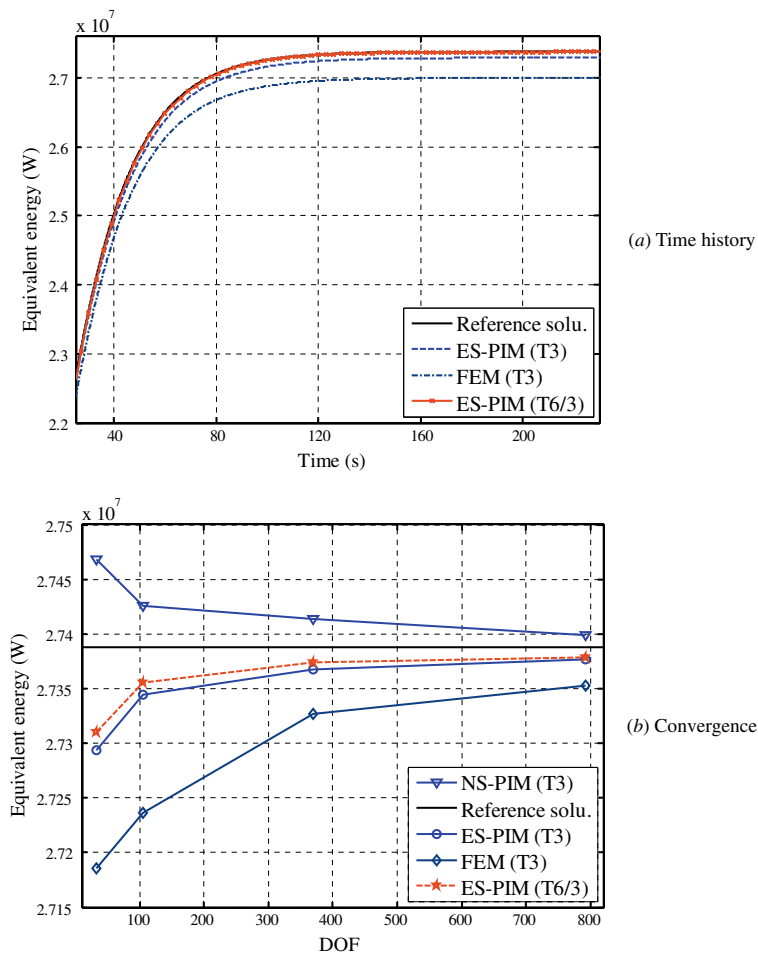


Fig. 3. The equivalent energy for the NS-PIM, present ES-PIM and linear FEM together with reference one.

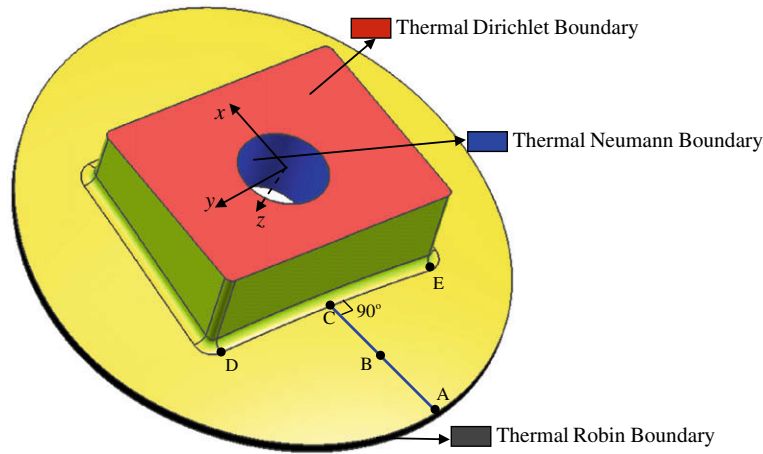


Fig. 4. An engine pedestal subjected to the Dirichlet, Neumann and Robin boundary conditions, respectively, on the baseplane, inner surface of installation hole, circumferential surface of the cap structure.

smoothed system [6,11]. As the analytical solutions of these complex problems are not available, reference solution is then obtained using the ABAQUS®, in which a very fine mesh with high-order cells is adopted. The equivalent energy norm for heat transfer model [5] is defined as

$$U_T = \int_{\Omega} \bar{\mathbf{g}}^T \mathbf{k} \bar{\mathbf{g}} d\Omega \quad (29)$$

where, in our current case, $\bar{\mathbf{g}}$ is the smoothed temperature gradient in Eq. (24).

4.1. 2D heat transfer beam

To verify the present ES-PIM formulation, a 2D heat transfer problem with mixed boundary conditions is first examined as illustrated in Fig. 2. In the computation, the parameters are taken as $k_1 = 50.0 \text{ W}/(\text{m}^\circ\text{C})$, $k_2 = 50.0 \text{ W}/(\text{m}^\circ\text{C})$, $h = 1500 \text{ W}/(\text{m}^2 \text{ }^\circ\text{C})$, $q_T = -4000 \text{ W}/\text{m}^2$, $T_r = 0 \text{ }^\circ\text{C}$, $Q_v = 0 \text{ W}/\text{m}^3$, $T_b = 200 \text{ }^\circ\text{C}$, $\rho = 3000 \text{ kg}/\text{m}^3$, $c = 50 \text{ J}/(\text{kg} \text{ }^\circ\text{C})$ and $T_{ini} = 25 \text{ }^\circ\text{C}$. In analysis of the transient state, the time increment is selected to $\Delta t = 0.1 \text{ s}$. The reference solution is obtained using ABAQUS® with a very fine mesh of 8241 nodes for comparison purposes.

It is well-known that the compatible FEM always obtains a lower bound of the exact solution in energy norm to elasticity problems due to its overly-stiff property. The important property of upper bound in equivalent energy has also been studied using the NS-PIM for 2D and 3D steady heat transfer [14–16]. To examine the ES-PIM convergence of equivalent energy of transient system, four models are created with 33, 105, 369 and 793 nodes. For comparison, NS-PIM and FEM using the same meshes are also used to compute the same problem.

Fig. 3a presents the time history of equivalent energy defined in Eq. (29). It is found that the linear ES-PIM model is more close to the reference one, compared with linear FEM model using the three-node triangular mesh. It can also be observed that the results of quadratic ES-PIM are in a very good agreement with the reference ones and are even better results than the linear model. Note that the transient system will arrive at the steady state in about $t = 160 \text{ s}$.

Fig. 3b further shows the convergence of energy solution when the system approaches steady at $t = 250 \text{ s}$. As expected from Fig. 3b, FEM and NS-PIM give lower and upper bound to the reference solution. ES-PIM models perform softer than the FEM but stiffer than the NS-PIM, which implies that more accurate solution can be obtained compared with the FEM. Compared with the linear ES-

PIM, the quadratic ES-PIM performs softer and provides results of a little better accuracy and higher convergence. This kind of insignificantly improved accuracy is mainly due to the discount effect on smoothing operation in higher order interpolations [8]. It is again seen that the present ES-PIM can provide a close-to-exact solution in equivalent energy form: it is much softer than the “overly-stiff” FEM and much stiffer than the “overly-soft” NS-PIM model. The important finding implies that the ES-PIM can be used to analyze time-dependent problems with much more accurate solutions in primary variable. In addition, better convergence can also be obtained compared with linear FEM.

4.2. A 3D engine pedestal

This section analyzes a real engine pedestal with very complex geometries, which is manufactured by the plasma deposition-layered technique [35]. The pedestal part is made of superalloy material, and detailed dimensions and processing parameters can be found in Ref. [42]. Fig. 4 is the illustration of the engine pedestal.

To examine the evolution of nodal temperature of the component, three points are sampled as shown in Fig. 4, in which points C and B are the midpoints of lines DE and CA, respectively. Some computational parameters are taken as $k_1 = 30.0 \text{ W}/(\text{m}^\circ\text{C})$,

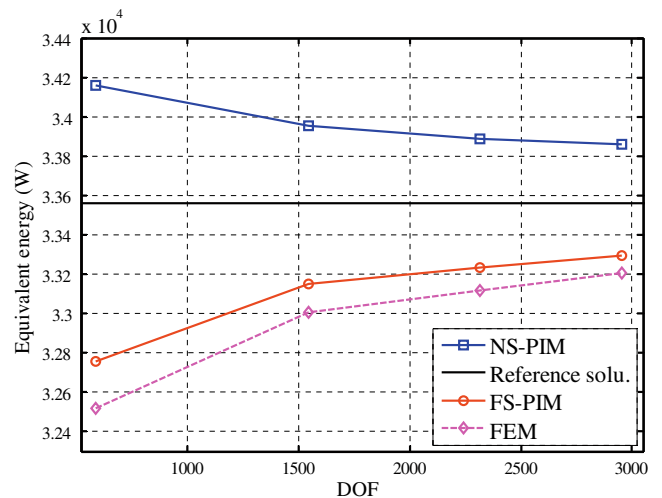


Fig. 5. Comparisons of equivalent energy obtained using present ES-PIM, NS-PIM and FEM based on the same tetrahedral mesh, together with the reference result.

$k_2 = 40.0 \text{ W/(m }^\circ\text{C)}$, $k_3 = 50.0 \text{ W/(m }^\circ\text{C)}$, $h = 1000 \text{ W/(m}^2 \text{ }^\circ\text{C)}$, $q_T = -6000 \text{ W/m}^2$, $T_T = 0 \text{ }^\circ\text{C}$, $Q_v = 0 \text{ W/m}^3$, $T_b = 500 \text{ }^\circ\text{C}$, $\Delta t = 0.0002 \text{ s}$, $c = 100 \text{ J/(kg }^\circ\text{C)}$ and $\rho = 3000 \text{ kg/m}^3$.

In 3D space, the smoothing operation on compatible temperature gradient is performed based on faces of the tetrahedrons and then the FS-PIM can be formulated. To confirm the FS-PIM's convergence of equivalent energy and the solution bounds, four sets of meshes are generated with irregularly scattered 587, 1543, 2315 and 2956 nodes, respectively, for the 3D part. Fig. 5

plots the energy solutions against the increasing of DOFs for FS-PIM, NS-PIM and FEM using the same meshes, together with the reference one obtained using a very fine mesh of 12,344 nodes.

As expected, the FEM model behaves overly-stiff and hence gives a lower bound solution, and NS-PIM behaves overly-soft and thus provides an upper bound solution, which has also been presented and proven [14–16,21]. The FS-PIM gives a very close-to-exact stiffness and hence the results of primary variables in matrix norm will be more accurate than those of the fully-compatible

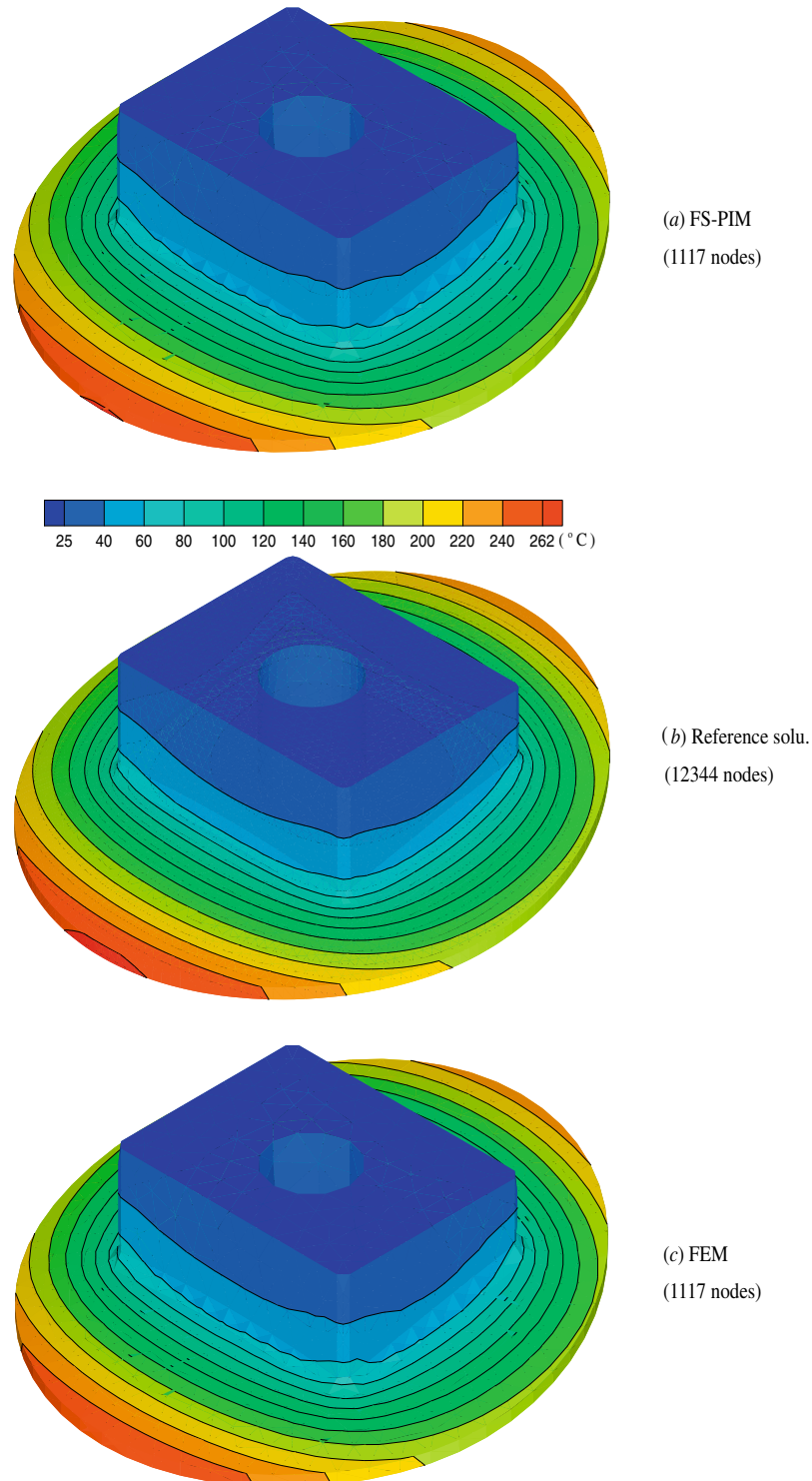


Fig. 6. Comparisons of computed temperature distributions for the cap part ($t = 20 \text{ s}$).

FEM. Again we find that the FS-PIM presents the comparative convergence in equivalent energy.

The following contours of Fig. 6 examine the accuracy of temperature distributions when the transient system arrives at the steady state at $t = 20$ s. It is observed that FS-PIM gives more accurate results than those of FEM using the same four-node tetrahedral mesh and linear shape functions. This finding will be further evaluated in the following Fig. 7 by checking the results at the three points.

Fig. 7 checks the numerical accuracy by plotting the time history of temperature at sample points A, B and C, for both FS-PIM and FEM using the same tetrahedral mesh. The numerical results are also compared with the reference solution obtained using a very fine mesh of 12,344 nodes with high-order cells.

It can be clearly seen that the temperatures obtained using FS-PIM at points A, B, and C are closer to the reference results than

those of linear FEM using the same mesh. It is also found that this system actually reaches the steady state when $t = 8$ s.

4.3. 3D manufacturing system

In those rapid manufacturing processes, such as the manufacturing using high energy density beam heat source of laser and plasma [32], metal components or structures experience drastic changes in temperature especially the critical region. This characteristic usually leads to extreme temperature gradient and hence produces undesired and unpredictable cracks and distortions in the components. Experimental study on these kinds of systems is very difficult, time-consuming and expensive to acquire detailed thermal and mechanical behaviors. Therefore, the need to numerically exploit and predict thermal responses of such special pro-

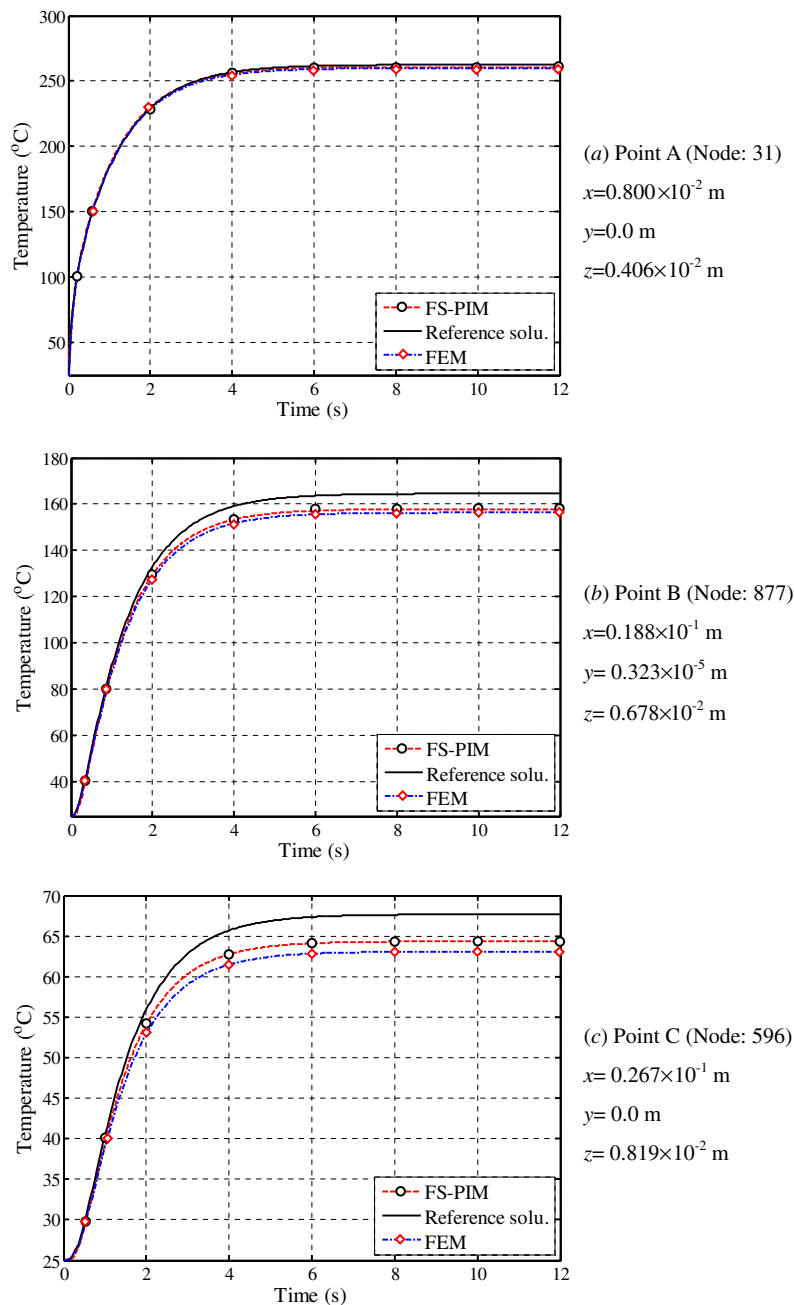


Fig. 7. Comparisons of temperature history at points A, B and C of the cap part ($t = 20$ s).

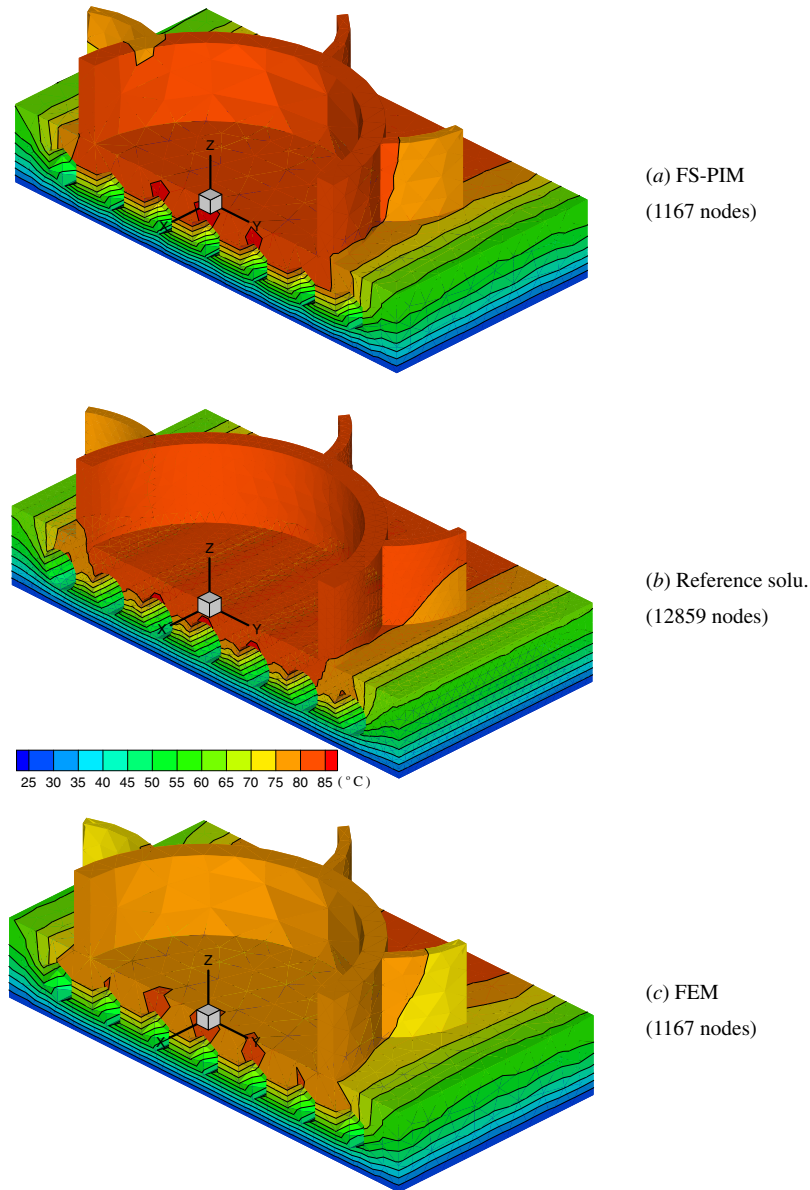


Fig. 9. Comparisons of computed steady temperature distributions ($t = 150$ s).

pose of evaluating the cooling effectiveness. This section focuses on studying the cooling and preheating effects, respectively, on deposited turbine and the substrate by tuning the water temperature T_b and convective heat transfer coefficient h that can be empirically computed [44] by the following equations:

$$Re = v_m D / \nu \quad (30)$$

$$Nu = 0.023 Re^{0.8} Pr^{0.34} \quad (31)$$

$$h_e = Nu k_b / D \quad (32)$$

in which D is the diameter of circular tube, v_m is mean flow velocity, ν is the kinematic viscosity of fluid, Re is the Reynolds number, Nu is the average Nusselt number, Pr is the Prandtl number, k_b is thermal conductivity of fluid.

To quantitatively evaluate the cooling system, we list two cases. One is to change the fluid velocity and the other is to control the bulk temperature.

Fig. 11 gives the temperature evolution of sample points B, D, E and G, under different velocity of fluid in Case 1 using the FS-PIM

with 1547 nodes. Note here that this system approaches the steady state at about 70 s.

It can be clearly found that: (a) the cooling water plays a very important role for rapidly cooling the deposited system in 10 s, as represented in Fig. 11a and c for the turbine and especially in Fig. 11b and d for the substrate; (b) the cooling water can take away the excessive heat energy originated from molten deposition in the scanning period; (c) the mean velocity of cooling water has much influence on cooling the substrate and hence on deposited turbine.

In practical manufacturing process, it is the “cooled” substrate that directly determines the cooling effects. Note that higher water velocity is difficult to control and usually gives rise to the excessive complexity in experiment setups and hence the increasing in cost. More importantly, the rapid solidification of deposited turbine also degrades the joint of deposition with the substrate. In the manufacturing, the deposited turbine needs to be cooled at desired temperature, generally about 600–800 °C during a period of 10 s [35]. Based on above considerations and results demonstrated in Fig. 11, the fluid velocity of 0.5 m/s is a preferable option.

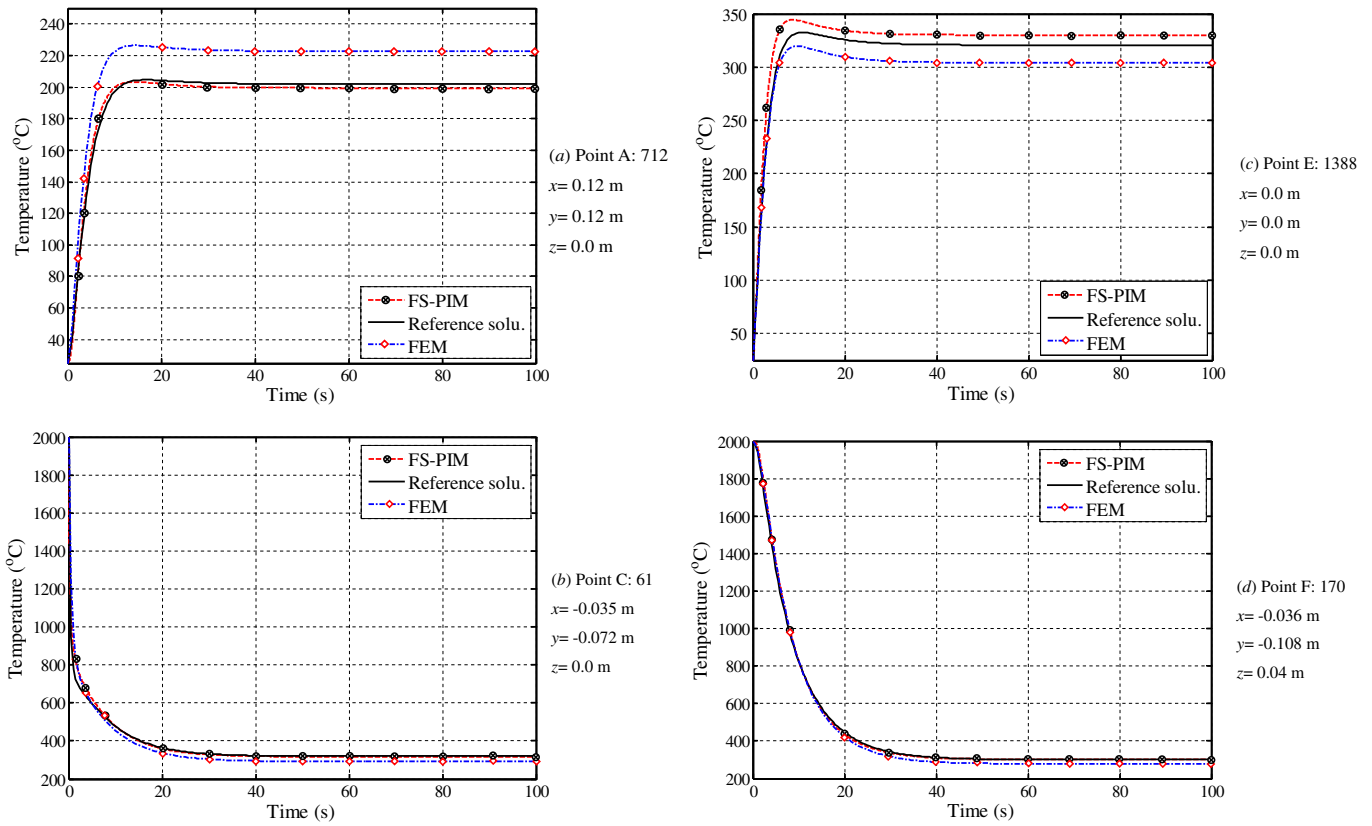


Fig. 10. Temperature variation with time of sample points (A, C, E and F).

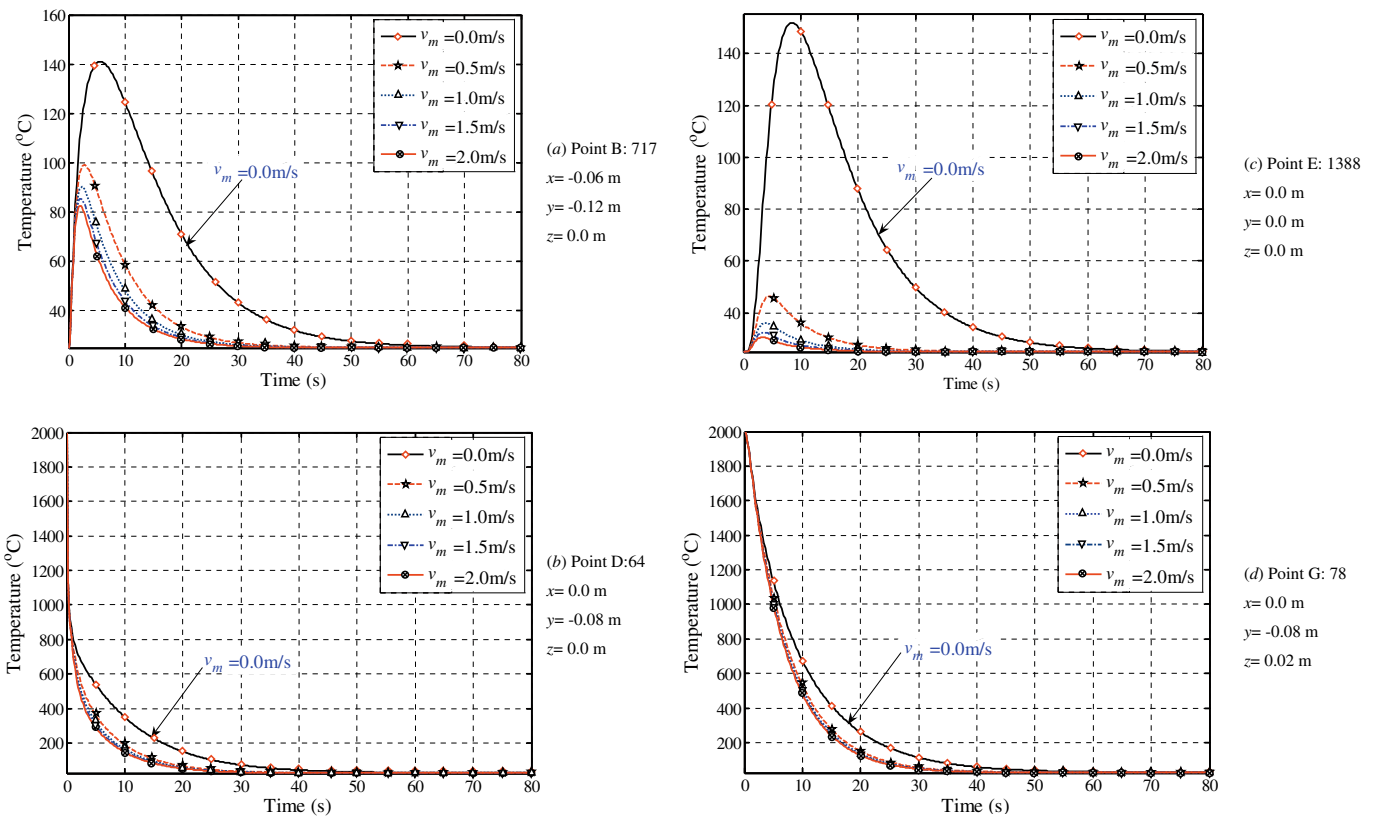


Fig. 11. Temperature evolutions for points B, D, E and G with the bulk temperature of $T_b = 25$ °C under different water velocity.

On the other hand, the substrate requires to be preheated for the perfect joint of substrate with molten metal powder. By providing the heated water, the cooling water can also be responsible for the preheating of substrate, which may replace the preheating scheme using a stove below the substrate presented in Ref. [35]. This is mainly because that the preheating using a stove is uncontrollable in practical manufacturing and leads to the deformation of CNC machine.

The following Fig. 12 analyzes the preheating effect of water temperature on substrate under the constant mean velocity of cooling water.

It can be found from Fig. 12 that: (a) the water temperature determines the temperature of steady state of system; (b) for preheating the substrate, the water temperature of $T_b = 40^\circ\text{C}$ is suitable and also capable of preventing the deformation of connected plastic tubes of cooling water; (c) $T_b = 40^\circ\text{C}$ is also acceptable for cooling the deposited turbine to $600\text{--}800^\circ\text{C}$ in 10 s; (d) the temperature of central region is lower than other section of the substrate.

In conclusion, there exists an optimal combination for bulk temperature and fluid velocity, which is selected as $T_b = 40^\circ\text{C}$ and $v_m = 0.5\text{ m/s}$ (the equivalent film convection coefficient of $h_e = 2637\text{ W}/(\text{m}^2\text{ }^\circ\text{C})$) from above analysis.

5. Conclusions

In this work, both ES-PIM and FS-PIM are formulated to, respectively, analyze 2D and 3D transient heat transfer problems with complex geometry. The accuracy and convergence in temperature and equivalent energy are examined in details through numerical examples. An important realistic cooling process of manufacturing system has been evaluated to obtain optimal cooling parameters in

both bulk temperature T_b and fluid velocity v_m . From this study, the following conclusions can be made:

1. The ES-PIM works very well with triangular and tetrahedral meshes that can be easily generated thanks to the softening effects provided by the generalized gradient smoothing technique. This approach is easy to implement as the standard FEM without introducing additional DOFs and parameters.
2. The ES-PIM can obtain a close-to-exact “stiffness” (conductance) that is much softer than the “overly-stiff” of FEM and much stiffer than the “overly-soft” NS-PIM, and hence applicable to transient heat transfer problems.
3. The ES-PIM models perform more softly than of the linear FEM and more stiffly than the NS-PIM, leading to more accurate temperature solutions than FEM using the same linear meshes.
4. Comparing to the linear FEM using the same mesh, the linear ES-PIM can achieve higher accuracy and better convergence in temperature and equivalent energy for both 2D and 3D problems with complicated geometry.
5. Using the FS-PIM, an important cooling system of the rapid direct manufacturing process has been analyzed, and an optional combination of the processing parameters has been found: $v_m = 0.5\text{ m/s}$ and $T_b = 40^\circ\text{C}$.

Meshfree methods, in general, require more CPU time compared with well-developed FEM for models of same DOFs [6,33]. The total DOFs of ES-PIM and that of the standard FEM are exactly the same when the same linear mesh is adopted, and hence the computational cost for the ES-PIM model and the FEM model are of the same order. Since the sparseness of ES-PIM models is 4/3 times of the FEM counterpart, ES-PIM takes about 1.7 times CPU time [15] in solving the system equations even when a bandwidth solved is used [41]. If an interactive solver is used, ES-PIM takes

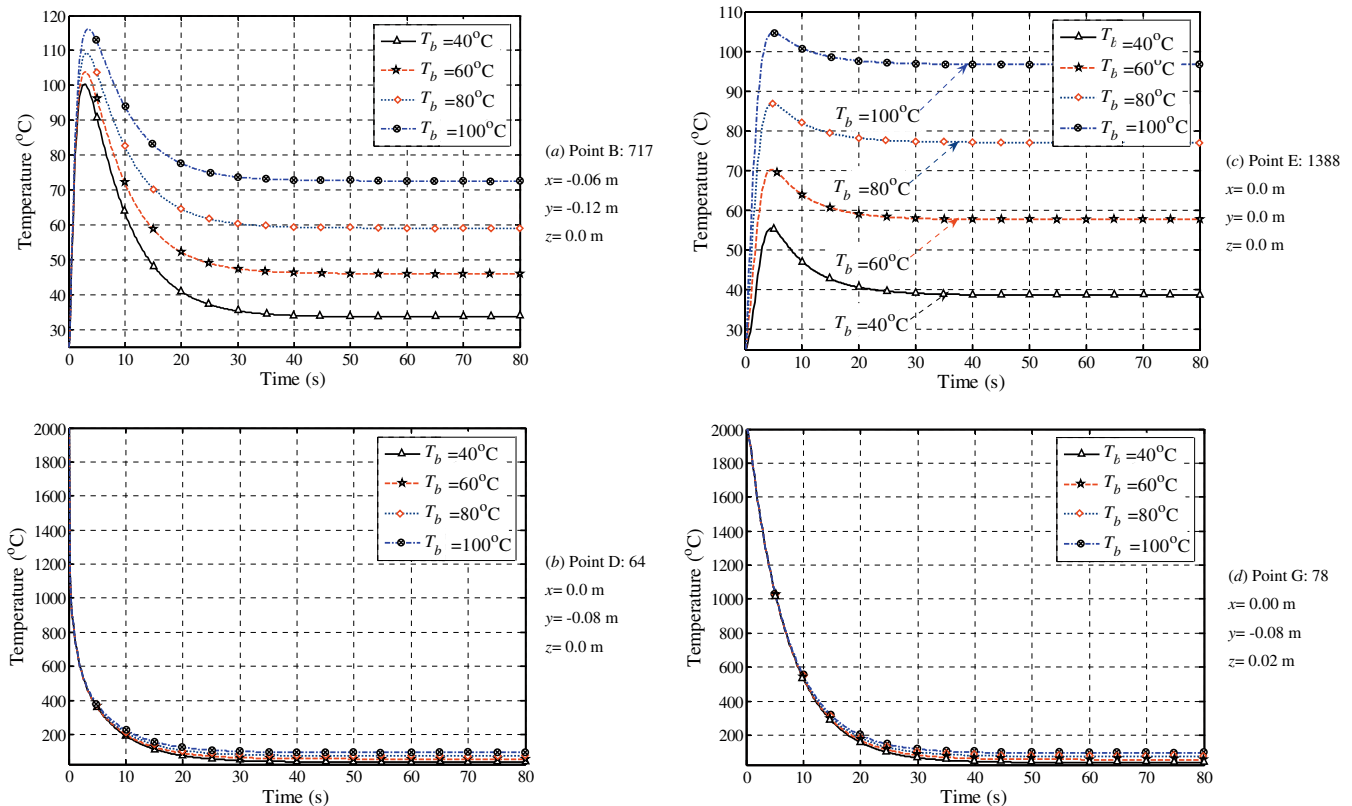


Fig. 12. Temperature evolutions for points B, D, E and G with water velocity of 0.5 m/s under different water temperature.

only about 1.3 times CPU time of the linear FEM. Note that the solution accuracy of linear ES-PIM using constant strain mesh is much better (about 10 times) than corresponding FEM using the same mesh. Therefore, in terms of computational efficiency (computation time for the same accuracy), the linear ES-PIM has been found superior to FEM by as much as 5–10 times and offers a very promising platform for practical problems.

Acknowledgements

This work is supported by the Ph.D. Project with No. GDBJ2009-025 and partially by A* Star, Singapore. It is also partially supported by the Science Fund Program of the State Key Laboratory of Advanced Design and Manufacturing for Vehicle Body. The authors also give sincerely thanks to the support of the Singapore-MIT Alliance (SMA), National University of Singapore.

References

- [1] R.W. Lewis, K. Morgan, H.R. Thomas, K.N. Seetharamu, *The Finite Element Method in Heat Transfer Analysis*, John Wiley & Sons, New York, 1996.
- [2] W.J. Minkowycz, E.M. Sparrow, J.Y. Murthy, *Handbook of Numerical Heat Transfer*, second ed., Wiley, Hoboken, NJ, 2006.
- [3] I.M. Smith, D.V. Griffiths, *Programming the Finite Element Method*, fourth ed., Wiley, Hoboken, NJ, 2004.
- [4] G.R. Liu, S.S. Quek, *Finite Element Method: A Practical Course*, Butterworth-Heinemann, Burlington, MA, 2003.
- [5] O.C. Zienkiewicz, R.L. Taylor, *The Finite Element Method*, fifth ed., Butterworth-Heinemann, Oxford, 2000.
- [6] G.R. Liu, *Meshfree Methods: Moving Beyond the Finite Element Method*, second ed., CRC Press, Boca Raton, USA, 2009.
- [7] G.R. Liu, G.Y. Zhang, K.Y. Dai, Y.Y. Wang, Z.H. Zhong, G.Y. Li, X. Han, A linearly conforming point interpolation method (LC-PIM) for 2D solid mechanics problems, *Int. J. Comput. Methods* 2 (2005) 645–665.
- [8] G.R. Liu, A G space theory and a weakened weak (W^2) form for a unified formulation of compatible and incompatible methods: Part I theory, *Int. J. Numer. Methods Eng* (2009), doi:10.1002/nme.2719.
- [9] G.R. Liu, G.Y. Zhang, Edge-based smoothed point interpolation methods, *Int. J. Comput. Methods* 5 (2008) 621–646.
- [10] I.V. Singh, Meshless EFG method in three-dimensional heat transfer problems: a numerical comparison, cost and error analysis, *Numer. Heat Transfer A Appl.* 46 (2004) 199–220.
- [11] P. Smolinski, T. Palmer, Procedures for multi-time step integration of element-free Galerkin method for diffusion problems, *Comput. Struct.* 77 (2000) 171–183.
- [12] H.K. Ching, J.K. Chen, Thermomechanical analysis of functionally graded composites under laser heating by the MLPG method, *CMES* 13 (2006) 199–217.
- [13] A.K. Chaniotis, D. Poulikakos, P. Koumoutsakos, Remeshed smoothed particle hydrodynamics for the simulation of viscous and heat conducting flows, *J. Comput. Phys.* 182 (2002) 67–90.
- [14] S.C. Wu, G.R. Liu, H.O. Zhang, G.Y. Zhang, A node-based smoothed point interpolation method (NS-PIM) for three-dimensional thermoelastic problems, *Numer. Heat Transfer A Appl.* 54 (2008) 1121–1147.
- [15] S.C. Wu, G.R. Liu, H.O. Zhang, X. Xu, Z.R. Li, A node-based smoothed point interpolation method (NS-PIM) for three-dimensional heat transfer problems, *Int. J. Therm. Sci.* 48 (2009) 1367–1376.
- [16] S.C. Wu, G.R. Liu, H.O. Zhang, G.Y. Zhang, A node-based smoothed point interpolation method (NS-PIM) for thermoelastic problems with solution bounds, *Int. J. Heat Mass Transfer* 52 (2008) 1464–1471.
- [17] G.R. Liu, Y.T. Gu, A point interpolation method for two-dimensional solids, *Int. J. Numer. Methods Eng.* 50 (2001) 937–951.
- [18] G.R. Liu, A generalized gradient smoothing technique and the smoothed bilinear form for Galerkin formulation of a wide class of computational methods, *Int. J. Comput. Methods* 5 (2008) 199–236.
- [19] J.S. Chen, C.T. Wu, S. Yoon, Y.A. You, A stabilized conforming nodal integration for Galerkin meshfree methods, *Int. J. Numer. Methods Eng.* 50 (2001) 435–466.
- [20] G.Y. Zhang, G.R. Liu, Y.Y. Wang, H.T. Huang, Z.H. Zhong, G.Y. Li, X. Han, A linearly conforming point interpolation method (LC-PIM) for three-dimensional elasticity problems, *Int. J. Numer. Methods Eng.* 72 (2007) 1524–1543.
- [21] G.R. Liu, G.Y. Zhang, Upper bound solution to elasticity problems: a unique property of the linearly conforming point interpolation method (LC-PIM), *Int. J. Numer. Methods Eng.* 74 (2008) 1128–1161.
- [22] G.R. Liu, T.T. Nguyen, H.X. Nguyen, K.Y. Lam, A node-based smoothed finite element method (NS-FEM) for upper bound solutions to solid mechanics problems, *Comput. Struct.* 87 (2009) 14–26.
- [23] G.R. Liu, K.Y. Dai, T.T. Nguyen, A smoothed finite element method for mechanics problems, *Comput. Mech.* 39 (2007) 859–877.
- [24] X.Y. Cui, G.R. Liu, G.Y. Li, X. Zhao, T. Nguyen-Thoi, G.Y. Sun, A smoothed finite element method (SFEM) for linear and geometrically nonlinear analysis of plates and shells, *CMES* 28 (2008) 109–125.
- [25] K.Y. Dai, G.R. Liu, T.T. Nguyen, An n -sided polygonal smoothed finite element method (nSFEM) for solid mechanics, *Finite Elem. Anal. Des.* 43 (2007) 847–860.
- [26] G.R. Liu, T.T. Nguyen, K.Y. Dai, K.Y. Lam, Theoretical aspects of the smoothed finite element method (SFEM), *Int. J. Numer. Methods Eng.* 71 (2007) 902–930.
- [27] G.R. Liu, T.T. Nguyen, K.Y. Lam, An edge-based smoothed finite element method (ES-FEM) for static, free and forced vibration analyses of solids, *J. Sound Vib.* 320 (2008) 1100–1130.
- [28] X.Y. Cui, G.R. Liu, G.Y. Li, G. Y. Zhang, G.Y. Sun, Elasto-plasticity analysis using edge-based smoothed finite element method (ES-FEM), *Int. J. Press. Vessels Pip.* 86 (2009) 711–718.
- [29] X.Y. Cui, G.R. Liu, G.Y. Li, G.Y. Zhang, G. Zheng, Analysis of plates and shells using an edge-based smoothed finite element method, *Comput. Mech.*, in press, doi: 10.1007/s00466-009-0429-9.
- [30] T.T. Nguyen, G.R. Liu, K.Y. Lam, G.Y. Zhang, A face-based smoothed finite element method (FS-FEM) for 3D linear and geometrically nonlinear solid mechanics problems using 4-node tetrahedral elements, *Int. J. Numer. Methods Eng.* 78 (2009) 324–353.
- [31] G.R. Liu, G.R. Zhang, A normed G space and weakened weak (W^2) formulation of a cell-based smoothed point interpolation method, *Int. J. Comput. Methods* 6 (1) (2009) 147–179.
- [32] X.Y. Cui, G.R. Liu, G.Y. Li, A cell-based smoothed radial point interpolation method (CS-RPIM) for static and free vibration of solids, *Eng. Anal. Boundary Elem.* 34 (2010) 144–157.
- [33] G.R. Liu, On a G space theory, *Int. J. Comput. Methods* 6 (2) (2009) 257–289.
- [34] Y. Jaluria, K.E. Torrance, *Computational Heat Transfer*, second ed., Taylor & Francis, London, 2003.
- [35] S.C. Wu, H.O. Zhang, G.L. Wang, Numerical and experimental evaluation of the temperature and stress fields during plasma deposition dieless manufacturing, in: K.P. Rajurkar (Ed.), *Proc. 15th ISEM*, Pittsburgh, USA, 2007, pp. 523–528.
- [36] G.R. Liu, Y.T. Gu, *An Introduction to Meshfree Methods and Their Programming*, Springer, Dordrecht, The Netherlands, 2005.
- [37] J.G. Wang, G.R. Liu, A point interpolation meshless method based on the radial basis functions, *Int. J. Numer. Methods Eng.* 54 (2002) 1623–1648.
- [38] G.Y. Zhang, G.R. Liu, T.T. Nguyen, C.X. Song, X. Han, Z.H. Zhong, G.Y. Li, The upper bound property for solid mechanics of the linearly conforming radial point interpolation method (LC-RPIM), *Int. J. Comput. Methods* 4 (2007) 521–541.
- [39] G.R. Liu, G.Y. Zhang, Y.Y. Wang, Z.H. Zhong, G.Y. Li, X. Han, A nodal integration technique for meshfree radial point interpolation method (NI-RPIM), *Int. J. Solids. Struct.* 44 (2007) 3840–3860.
- [40] M.N. Ozisik, *Heat Conduction*, second ed., Wiley Press, Singapore, 1993.
- [41] S.L. Xu, *FORTRAN Algorithms and Program*, second ed., Tsinghua University Publisher, Beijing, 1995.
- [42] G.L. Wang, S.C. Wu, H.O. Zhang, Numerical simulation of temperature field on complicated parts during plasma deposition dieless manufacturing, *Trans. Chin. Welding Inst.* 28 (2007) 49–52.
- [43] Y.C. Lin, K.H. Lee, Effect of preheating on the residual stress in Type 304 stainless steel weldment, *J. Mater. Process. Tech.* 63 (1997) 797–801.
- [44] S. Kakac, Y. Yener, *Convective Heat Transfer*, second ed., CRC Press, Boca Raton, USA, 1995.